Complete 1D Continuum Model for a Pantographic Beam by Asymptotic Homogenization from Discrete Elements with Shear Deformation Measure

Maximilian Stilz, Francesco Dell'Isola, Stefan Hiermaier

Complete 1D Continuum Model for a Pantographic Beam by Asymptotic Homogenization from Discrete Elements with Shear Deformation Measure

Maximilian Stilz[a], Francesco dell'Isola[b], Stefan Hiermaier[a,c]

[a]INATECH, University of Freiburg, Freiburg, Germany
[b]Department of Civil, Construction-Architecture and Environmental Engineering, University of L'Aquila, L'Aquila, Italy
[c]Fraunhofer Institute for High-Speed Dynamics, Ernst-Mach Institut, EMI, Freiburg, Germany

Abstract

Starting from a discrete model of a pantographic beam based on beam elements with 6 DOF in 2D space, 2 translational and 1 rotational for each end node, and proposing an energy quadratic in elongation, shear, bending and torsion deformation measures, we find by asymptotic homogenization a model of a complete 1D second gradient continuum. Compared to previous models, the discrete model of the present work includes shear deformation by considering the beam element's end nodes relative orientation. The resulting continuum model differs in a stiffness coefficient stemming from the shear deformation, but it coincides in the limit of shear stiff elements.

1. Introduction

Analyzing structural deformation of materials composed of discrete sub-elements can be tedious and computationally challenging as many degrees of freedom have to be considered [1, 2, 3]. If the structure in question has some form of periodicity, a homogenization procedure might be applicable to achieve a reduced order continuum model [4, 5, 6, 7, 8, 9]. Microstructures which got special attention in recent years are pantographic structures [5, 10, 11, 12] as their continuum equivalents go beyond the scope of classic continuum mechanics as they may show behavior that is well attributed to a dependency on the second derivative of displacement. These effects become especially (but not exclusively) prevalent if the beam structural elements are conjoined by perfect hinges [13]. Under certain boundary conditions, these perfect rotational connections can introduce zero energy deformation modes [14, 15]. Pantographic structures show high compliance in experiments and the derived continuum models are suitable predictors [16, 17] while at the same time due to slender beams and small joints made by 3D printing [18], damage phenomena have been studied [19, 20, 21, 22] to extend these models.

One particular pantographic structure is the pantographic beam [16, 23, 4, 24], a series of beam elements at $\frac{\pi}{2}$ angle to each other and hinge joined by e.g. rotational springs along a center line. In previous works [4], a homogenization has been performed based on a Hencky-type spring model with extensible and rotational springs. Through defining an identification of the micro parameters with macro fields, a variational asymptotic procedure led to a continuum model with a deformation energy dependent on curvature as well as gradient of stretch. The model performs well in comparison to the discrete model [25].

The former model and most other models for pantographic structures do not take into account the shear deformability of the sub-structural elements in homogenization approaches. Discrete shear deformable beam element models are available [26] and have been applied to beams and pivots of pantographic sheets [27, 28, 29]. Although, both this and former models result in a nonlinear beam model that has an internal energy density with dependency on the curvature and stretch as well as gradient of stretch, therefore on all second derivatives of displacement. For numerical treatment of this kind of beam, director based descriptions [30, 31] or methods aimed at kirchhoff rods [32, 33] should be extendable.

In this work we start from a discrete model that extends the Hencky-model from [4] with a shear deformation measure by distinguishing between the angle of a beam element's end node and its tangent direction described in Section 2. For simplicity, we choose all discrete deformation measures to be linear in either displacement or angles, respectively, and energies quadratic in these deformation measures. The thus formulated discrete model is presented in Section 2.1. We arrive at a model with three nodes per unit cell with two displacement and two rotational degrees of freedom. To reduce the degrees of freedom, we perform a first condensation in Section 2.2 where through energy minimization the four angles of the auxiliary points could be expressed by other kinematic descriptors. In Section 3 and subsections the homogenization procedure is documented. The micro-macro identification is described in Section 3.1 and followed by the expansion of kinematic descriptors to decouple them from the inner lengths $\boldsymbol{\varepsilon}$ in Section 3.2. Subsequently, we introduce the stiffness rescaling in Section 3.3 and perform a second condensation in Section 3.7. After complete expan-

sion in terms of ε, a continuum energy density is proposed in Section 4. A comparison in Section 4.1 to [4] shows a combined shear and bending stiffness coefficient in place of only a bending coefficient and an agreement in the limit of shear stiff beam elements. Due to the similarities of the resulting homogenized energies no simulations were performed in this work. A detailed analysis in comparison to this and further discrete models will follow in future work.

2. Discrete Model

The discrete model is based on beam elements whose configuration is based on the position of its two end nodes e.g. P_i, O_i and their angles e.g. ψ^{P_i}, ψ^{O_i}. The angles are defined in relation to a straight reference configuration as seen in Figure 1. We define two types of connections between two beam elements. First, we can rigidly connect two of the beam elements and fix their nodal positions and angle to create a longer beam element. Secondly, we can connect the positions of two nodes but do not fix their angles. With these rules we can build a pantographic beam with two families of fibers, one family which is rotated $+\frac{\pi}{2}$ and the other $-\frac{\pi}{2}$ with respect to its central line in the reference configuration. Beams of the same family meeting in a point P_i have a rigid connection while beams from different families are only connected by displacement but not rotation. For example $\psi^{O_i^+}$ defines the angle of the end node of the beam from P_i to O_i with length $l^{P_iO_i}$ while $\psi^{O_i^-}$ is the angle of the first node of the beam from O_i to P_{i+1} with length $l^{O_iP_{i+1}}$ (See Figure 2 and 3 for details). The centerline of the pantographic beam shall be along the points P_i while O_i and Q_i are called auxiliary points in the following.
The geometric angles φ, introduced in Figure 2, can be expressed by the law of cosine in terms of the distance between points l:

$$\cos\varphi^{P_iO_i} = \frac{\left(l^{P_iO_i}\right)^2 + \left(l^{P_iP_{i+1}}\right)^2 - \left(l^{O_iP_{i+1}}\right)^2}{2l^{P_iO_i}l^{P_iP_{i+1}}} , \tag{1}$$

$$\cos\varphi^{O_iP_{i+1}} = \frac{\left(l^{O_iP_{i+1}}\right)^2 + \left(l^{P_iP_{i+1}}\right)^2 - \left(l^{P_iO_i}\right)^2}{2l^{O_iP_{i+1}}l^{P_iP_{i+1}}} , \tag{2}$$

$$\cos\varphi^{P_iQ_i} = \frac{\left(l^{P_iQ_i}\right)^2 + \left(l^{P_iP_{i+1}}\right)^2 - \left(l^{Q_iP_i}\right)^2}{2l^{P_iQ_i}l^{P_iP_{i+1}}} , \tag{3}$$

$$\cos\varphi^{Q_iP_{i+1}} = \frac{\left(l^{Q_iP_{i+1}}\right)^2 + \left(l^{P_iP_{i+1}}\right)^2 - \left(l^{P_iQ_i}\right)^2}{2l^{Q_iP_{i+1}}l^{P_iP_{i+1}}} . \tag{4}$$

2.1. Discrete Energy

For a pantographic beam with a reference configuration as in Figure 1 of length L we can define the complete energy as a sum of the elongation, shear and bending energies of each beam element and the torsional energy of the springs between two different fiber families. We define for a beam element the extensional stiffness k_e, the shear stiffness k_γ, the bending stiffness k_f and for rotational springs between two fiber families at one node the torsional stiffness k_t. We then propose the following energy contributions:

Elongation

The energy defined using l as a measure for elongation, which can be seen as a first order approximation for small deformations as the true beam length does also depend on the angles ψ. We propose the elongation energy as

$$W_e = \sum_i W_e^{P_iO_i} + W_e^{O_iP_{i+1}} + W_e^{P_iQ_i} + W_e^{Q_iP_{i+1}} , \tag{5}$$

$$W_e^{P_iO_i} = \frac{1}{2}k_e\left(l^{P_iO_i} - \frac{\varepsilon}{\sqrt{2}}\right)^2 , \tag{6}$$

$$W_e^{O_iP_{i+1}} = \frac{1}{2}k_e\left(l^{O_iP_{i+1}} - \frac{\varepsilon}{\sqrt{2}}\right)^2 , \tag{7}$$

$$W_e^{P_iQ_i} = \frac{1}{2}k_e\left(l^{P_iQ_i} - \frac{\varepsilon}{\sqrt{2}}\right)^2 , \tag{8}$$

$$W_e^{Q_iP_{i+1}} = \frac{1}{2}k_e\left(l^{Q_iP_{i+1}} - \frac{\varepsilon}{\sqrt{2}}\right)^2 . \tag{9}$$

Shear

We define the shear deformation measure as the sum of the angles of a beam segment. This measure is the linearized version for small angles of the deformation measure for pivots in [29]. Therefore, we conjecture the shear energy as

$$W_\gamma = \sum_i W_\gamma^{P_iO_i} + W_\gamma^{O_iP_{i+1}} + W_\gamma^{P_iQ_i} + W_\gamma^{Q_iP_{i+1}} , \tag{10}$$

$$W_\gamma^{P_iO_i} = \frac{1}{2}k_\gamma\varepsilon^2\left(\frac{\pi}{4} - \vartheta_i - \varphi^{P_iO_i} + \frac{1}{2}\left(\psi^{P_i^+} + \psi^{O_i^+}\right)\right)^2 , \tag{11}$$

$$W_\gamma^{P_iQ_i} = \frac{1}{2}k_\gamma\varepsilon^2\left(-\frac{\pi}{4} - \vartheta_i + \varphi^{P_iQ_i} + \frac{1}{2}\left(\psi^{P_i^-} + \psi^{Q_i^-}\right)\right)^2 , \tag{12}$$

$$W_\gamma^{Q_iP_{i+1}} = \frac{1}{2}k_\gamma\varepsilon^2\left(\frac{\pi}{4} - \vartheta_i - \varphi^{Q_iP_{i+1}} + \frac{1}{2}\left(\psi^{Q_i^+} + \psi^{P_{i+1}^+}\right)\right)^2 , \tag{13}$$

$$W_\gamma^{O_iP_{i+1}} = \frac{1}{2}k_\gamma\varepsilon^2\left(-\frac{\pi}{4} - \vartheta_i + \varphi^{O_iP_{i+1}} + \frac{1}{2}\left(\psi^{P_{i+1}^-} + \psi^{O_i^-}\right)\right)^2 . \tag{14}$$

The angles φ and ϑ correct for rigid rotations from the perspective of the affected beam as the angles ψ are relative to the reference configuration.

Bending

Bending deformation is measured as the difference of the two angles of a beam segment with

$$W_f = \sum_i W_f^{P_iO_i} + W_f^{O_iP_{i+1}} + W_f^{P_iQ_i} + W_f^{Q_iP_{i+1}} , \tag{15}$$

$$W_f^{P_iO_i} = \frac{1}{2}k_f\left(\psi^{O_i^+} - \psi^{P_i^+}\right)^2 , \tag{16}$$

$$W_f^{O_iP_{i+1}} = \frac{1}{2}k_f\left(\psi^{P_{i+1}^-} - \psi^{O_i^-}\right)^2 , \tag{17}$$

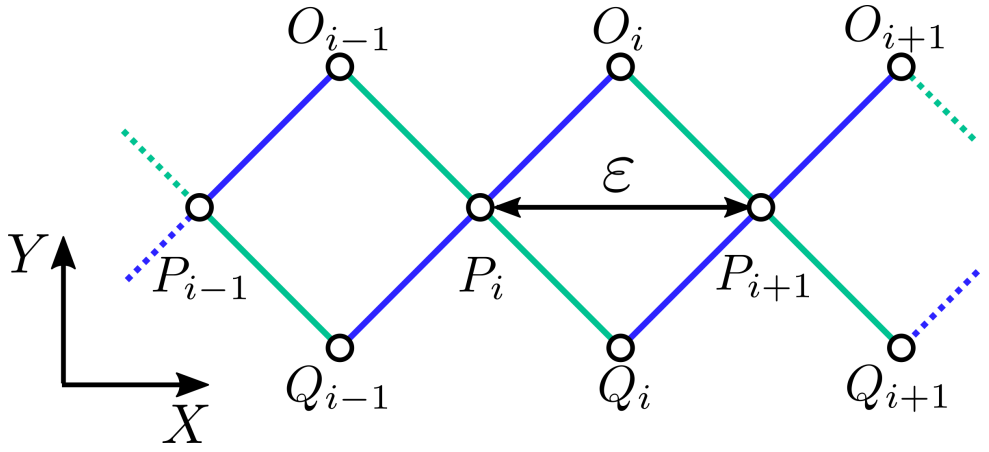

Figure 1: Section of the pantographic beam showing the two beam families in blue and green. For every center line point P_i there are two auxiliary points O_i and Q_i. The parameter ε gives the distance between two points P_i and P_{i+1} in the reference configuration and therefore serves as a periodicity length.

$$W_f^{P_iQ_i} = \frac{1}{2}k_f\left(\psi^{Q_i^-} - \psi^{P_i^-}\right)^2 , \tag{18}$$

$$W_f^{Q_iP_{i+1}} = \frac{1}{2}k_f\left(\psi^{P_{i+1}^+} - \psi^{Q_i^+}\right)^2 . \tag{19}$$

Pivot torsion

The difference of the two angles in one point define the torsional energy of the connection between the two beam families. We only consider torsion in the auxiliary points for better comparison with [24] but an additional term for the torsion in the center line points could be easily added.

$$W_t = \sum_i W_t^{O_i} + W_t^{Q_i} , \tag{20}$$

$$W_t^{O_i} = \frac{1}{2}k_t\left(\psi^{O_i^+} - \psi^{O_i^-}\right)^2 , \tag{21}$$

$$W_t^{Q_i} = \frac{1}{2}k_t\left(\psi^{Q_i^+} - \psi^{Q_i^-}\right)^2 . \tag{22}$$

2.2. First Condensation

Some inner degrees of freedom can be directly removed by means of energy minimization in the discrete model. This is the case for the angles of the auxiliary points $\psi^{O_i^\pm}$ and $\psi^{Q_i^\pm}$. We find that

$$\frac{\partial W_{\text{tot}}}{\partial \psi^{O_i^+}} \stackrel{!}{=} 0 \tag{23}$$

$$\begin{aligned}\Rightarrow \psi^{O_i^+} = {} & \frac{1}{2(4k_f+\varepsilon^2k_\gamma)(4k_f+\varepsilon^2k_\gamma+8k_t)} \\ & \Big[\left(32k_f^2-2k_\gamma^2\right)\psi^{P_i^+} \\ & +\left(32k_fk_t-8k_\gamma k_t\right)\left(\psi^{P_i^+}+\psi^{P_{i+1}^-}\right) \\ & +\left(4k_fk_\gamma+k_\gamma^2\right)\left(4\vartheta_i-\pi+4\varphi^{P_iO_i}\right) \\ & +16k_\gamma k_t\left(2\vartheta_i+\varphi^{P_iO_i}-\varphi^{O_iP_{i+1}}\right)\Big] .\end{aligned} \tag{24}$$

3. Homogenization Procedure

3.1. Micro-macro Identification

We identify the centerline of the pantographic beam in the limit for small ε as a 1D continuum with arc length $s \in [0, L]$ and a placement function $\boldsymbol{\chi} : [0, L] \mapsto \mathbb{R}^2$. $\boldsymbol{\chi}$ maps s into the Euclidean plane. In the framework of the asymptotic expansion in orders of ε neighboring points $\boldsymbol{p}_{i+1}$ are then estimated through

$$\boldsymbol{p}_i = \boldsymbol{\chi}(s_i) , \tag{25}$$

$$\boldsymbol{p}_{i+1} = \boldsymbol{\chi}(s_{i+1}) = \boldsymbol{\chi}(s_i) + \varepsilon\boldsymbol{\chi}'(s_i) + \frac{\varepsilon^2}{2}\boldsymbol{\chi}''(s_i) + O(\varepsilon^3) . \tag{26}$$

We also introduce the macro fields $\psi^{P^\pm} : [0, L] \mapsto [-\pi, \pi]$ and expansions for the angles at the nodes P_i

$$\psi^{P_i^\pm} = \psi^{P^\pm}(s_i) , \tag{27}$$

$$\psi^{P_{i+1}^\pm} = \psi^{P^\pm}(s_i) + \varepsilon\left(\psi^{P^\pm}\right)'(s_i) + O(\varepsilon^2) . \tag{28}$$

Similarly, for the placement angle we define the field $\vartheta : [0, L] \mapsto [-\pi, \pi]$ with

$$\vartheta_i = \vartheta(s_i) , \tag{29}$$

$$\vartheta_{i+1} = \vartheta(s_i) + \varepsilon\vartheta'(s_i) + O(\varepsilon^2) , \tag{30}$$

and for the beam lengths $l^{AB} : [0, L] \mapsto \mathbb{R}^+$ e.g.

$$l^{P_iO_i} = l^{PO}(s_i) , \tag{31}$$

$$l^{O_iP_{i+1}} = l^{OP}(s_i) . \tag{32}$$

3.2. Expansion of the kinematic descriptors

The angles $\psi^{P^\pm}$ may still depend on ε and we therefore introduce the asymptotic expansions

$$\psi^{P^\pm}(s_i) = \psi_0^{P^\pm}(s_i) + \varepsilon\psi_1^{P^\pm}(s_i) + O(\varepsilon^2) , \tag{33}$$

$$\psi^{P^\pm}(s_{i+1}) = \psi_0^{P^\pm}(s_{i+1}) + \varepsilon\psi_1^{P^\pm}(s_{i+1}) , \tag{34}$$

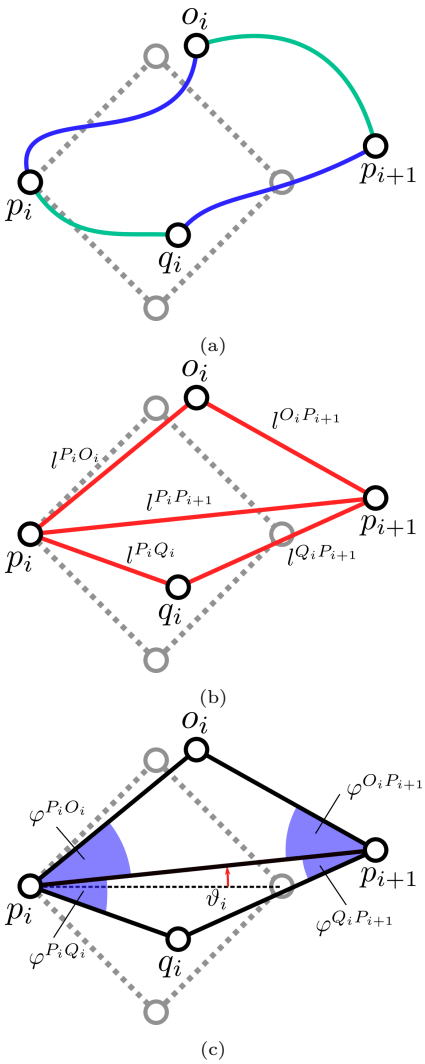

Figure 2: Geometric properties shown for a deformed unit cell. The reference configuration is shown as dotted lines. (a): Deformed beams and displaced nodes. (b): Distance between nodes l used as a measure for elongation deformation. (c): Geometric angles φ and ϑ to determine rigid rotations.

$$= \psi_0^{P^\pm}(s_i) + \varepsilon\left[\left(\psi_0^{P^\pm}\right)'(s_i) + \psi_1^{P^\pm}(s_i)\right] + O(\varepsilon^2) \ . \quad (35)$$

Similarly, we expand the lengths of the beams with $\tilde{l}^{AB} : [0, L] \mapsto \mathbb{R}$ to

$$l^{PO}(s_i) = \frac{\varepsilon}{\sqrt{2}} + \varepsilon^2 \tilde{l}^{PO}(s_i) + O(\varepsilon^3) \ , \quad (36)$$

$$l^{PQ}(s_i) = \frac{\varepsilon}{\sqrt{2}} + \varepsilon^2 \tilde{l}^{PQ}(s_i) + O(\varepsilon^3) \ , \quad (37)$$

$$l^{OP}(s_i) = \frac{\varepsilon}{\sqrt{2}} + \varepsilon^2 \tilde{l}^{OP}(s_i) + O(\varepsilon^3) \ , \quad (38)$$

$$l^{QP}(s_i) = \frac{\varepsilon}{\sqrt{2}} + \varepsilon^2 \tilde{l}^{QP}(s_i) + O(\varepsilon^3) \ , \quad (39)$$

and the distance of neighboring nodes

$$l^{P_iP_{i+1}} = \|\boldsymbol{p}_{i+1} - \boldsymbol{p}_i\| = \|\boldsymbol{\chi}(s_{i+1}) - \boldsymbol{\chi}(s_i)\| \quad (40)$$

$$= \varepsilon\|\boldsymbol{\chi}'(s_i)\| + \frac{\varepsilon^2}{2}\frac{\boldsymbol{\chi}'(s_i)\cdot\boldsymbol{\chi}''(s_i)}{\|\boldsymbol{\chi}'(s_i)\|} + O(\varepsilon^3) \quad (41)$$

$$= \varepsilon\rho(s_i) + \frac{\varepsilon^2}{2}\rho'(s_i) + O(\varepsilon^3) \ , \quad (42)$$

with $\rho(s_i) = \|\boldsymbol{\chi}'(s_i)\|$ as the stretch of the centerline.

This results, besides the placement function, in a set of the kinematic descriptors $\psi_0^{P^\pm}$, $\psi_1^{P^\pm}$, $\tilde{l}^{PO}$, $\tilde{l}^{PQ}$, $\tilde{l}^{OP}$, $\tilde{l}^{QP}$ that are independent of ε. Before further identification between the placement function and these descriptors is possible, we need to analyze the dependency of the stiffness coefficients on the size parameter ε to propose a complete asymptotic expansion of the energy.

3.3. Stiffness rescaling

The stiffnesses k_c generally also depend on ε as they are coupled to the dimensions of the discrete beams. We therefore propose a rescaling of these stiffnesses with

$$k_c \to \varepsilon^{\alpha_c} K_c \ , \quad (43)$$

with $\alpha_c \in \mathbb{Z}$.

We do not claim that there is any general rule for rescaling. However, every rescaling can bring a different continuum energy with additional kinematic conditions.

3.3.1. Rescaling Conjecture

We propose the following heuristic rescaling

$$k_e \to \varepsilon^{-3} K_e, \quad k_\gamma \to \varepsilon^{-3} K_\gamma, \quad k_f \to \varepsilon^{-1} K_f, \quad k_t \to \varepsilon K_t \ . \quad (44)$$

3.4. Expansion of the discrete energy

If we substitute the expansions, rescaling and condensation into the discrete energy, each energy contribution $c \in \{e, \gamma, f, t\}$ has the following form

$$W_c = \sum_{\beta\in\mathbb{Z}} \varepsilon^\beta K_c w_c^{(\beta)} = \sum_{\beta\in\mathbb{Z}} \varepsilon^\beta W_c^{(\beta)} \ , \quad (45)$$

$$W_{\text{tot}} = \sum_{\beta\in\mathbb{Z}} \varepsilon^\beta W_{\text{tot}}^{(\beta)} = \sum_{\beta\in\mathbb{Z}} \sum_c \varepsilon^\beta W_c^{(\beta)} \ , \quad (46)$$

where $w_c^{(\beta)}$ are functions of the kinematic descriptors and their derivatives but independent of ε. In the continuum limit the total energy has the form

$$\mathcal{W}_{\text{tot}} = \lim_{\varepsilon\to 0} W_{\text{tot}} = \lim_{\varepsilon\to 0} \sum_{\beta\in\mathbb{Z}} \varepsilon^\beta W_{\text{tot}}^{(\beta)} \ . \quad (47)$$

For all $\beta < 1$ and $W_{tot}^{(\beta)} \neq 0$ the contribution diverges in the limit. For $\beta > 1$ all contributions vanish in the limit. Therefore, we get additional kinematic conditions in the former case.

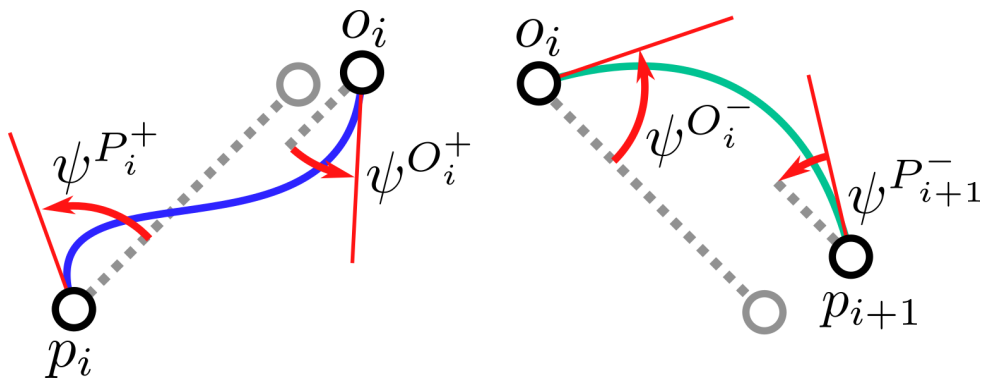

Figure 3: Beam angles ψ shown for the two families of beams. There are two angles for every node as there are always two beams. To calculate the true rotation angle of a beam node with respect to its reference configuration we need all three angles φ, θ and ψ to correct rigid rotations of the beam.

3.5. Kinematic constraints

The expansion was handled with the computer algebra software Wolfram Mathematica [34]. We find non-zero diverging contributions for $\beta = -1$ and $\beta = 0$ (see Appendix A for details). For them to vanish we get constraints for two kinematic descriptors with

$$W_{\text{tot}}^{(-1)} \stackrel{!}{=} 0 \tag{48}$$

$$W_{\text{tot}}^{(0)} \stackrel{!}{=} 0 \tag{49}$$

$$\Rightarrow \psi_0^{P^+}(s_i) = \vartheta(s_i) + \arccos\left(\frac{\rho(s_i)}{2}\right) - \frac{\pi}{4} \tag{50}$$

$$\Rightarrow \psi_0^{P^-}(s_i) = \vartheta(s_i) - \arccos\left(\frac{\rho(s_i)}{2}\right) + \frac{\pi}{4} \,. \tag{51}$$

3.6. Energy density

After removing all diverging terms, we are left with

$$\mathcal{W}_{\text{tot}} = \lim_{\varepsilon\to 0}\sum_{\beta}\varepsilon^{\beta}W_{\text{tot}}^{(\beta)} = \lim_{\varepsilon\to 0}\sum_{i}\varepsilon W_{i,\text{tot}}^{(1)} = \int_{\Omega} w_{\text{tot}}(s)\mathrm{d}s \tag{52}$$

where $w_{\text{tot}}(s)$ is the macro field energy density of the discrete energy per unit cell length ε with

$$w_{\text{tot}}(s_i) = W_{i,\text{tot}}^{(1)} \,. \tag{53}$$

3.7. Second Condensation

The remaining kinematic descriptors that stem from the micro kinematics can be identified with the macro kinematic descriptors by minimizing the energy density w_{tot} with respect to $\bar{l}^{AB}$ and $\psi_1^{P^\pm}$. We find stationary points for

$$\bar{l}^{PO} = 2\sqrt{2}\rho\left(-C_1(\rho)\rho' + C_2(\rho)\vartheta'\right) \,, \tag{54}$$

$$\bar{l}^{PQ} = 2\sqrt{2}\rho\left(-C_1(\rho)\rho' - C_2(\rho)\vartheta'\right) \,, \tag{55}$$

$$\bar{l}^{OP} = 2\sqrt{2}\rho\left(C_1(\rho)\rho' + C_2(\rho)\vartheta'\right) \,, \tag{56}$$

$$\bar{l}^{QP} = 2\sqrt{2}\rho\left(C_1(\rho)\rho' - C_2(\rho)\vartheta'\right) \,, \tag{57}$$

$$\psi_1^{P^+} = -\frac{1}{2}\vartheta' \,, \tag{58}$$

$$\psi_1^{P^-} = -\frac{1}{2}\vartheta' \tag{59}$$

with

$$C_1(\rho) = \frac{K_{f\gamma}}{8\left(2-\rho^2\right)K_{f\gamma} + \rho^2 K_e} \,, \tag{60}$$

$$C_2(\rho) = \frac{\sqrt{2-\rho^2}K_{f\gamma}}{8\rho^2 K_{f\gamma} + \left(2-\rho^2\right)K_e} \,, \tag{61}$$

$$K_{f\gamma} = \frac{K_f K_\gamma}{4K_f + K_\gamma} \,. \tag{62}$$

4. Macro Model

In the continuum limit for $\varepsilon \to 0$, we identify the discrete variables with their macro fields and find the total internal energy of the pantographic beam with all condensations and kinematic conditions in the form

$$\mathcal{W}_{tot} = \int_0^L f(\rho)\left(\rho'\right)^2 + g(\rho)\left(\vartheta'\right)^2 + h(\rho)\ \mathrm{d}s \,, \tag{63}$$

with

$$f(\rho) = C_1(\rho)\frac{\rho K_e}{\sqrt{2}\left(2-\rho^2\right)} \,, \tag{64}$$

$$g(\rho) = C_2(\rho)\frac{\left(2-\rho^2\right)K_e}{\sqrt{2}\rho\sqrt{2-\rho^2}} \,, \tag{65}$$

$$h(\rho) = K_t\left[\frac{\pi}{2} - 2\arccos\left(\frac{\rho}{\sqrt{2}}\right)\right]^2 \,. \tag{66}$$

4.1. Limit Case

In the limit for shear stiff beams with $K_\gamma \to \infty$ we find

$$K_{f\gamma} \stackrel{K_\gamma\to\infty}{=} K_f \,, \tag{67}$$

$$f(\rho) \stackrel{K_\gamma\to\infty}{=} \frac{2\rho^2 K_f K_e}{\left(2-\rho^2\right)\left[8\left(2-\rho^2\right)K_f + \rho^2 K_e\right]} \,, \tag{68}$$

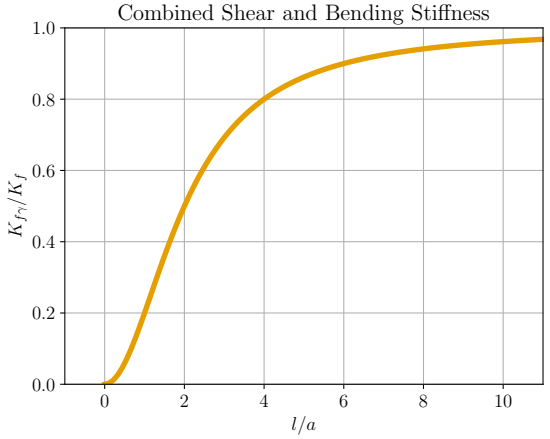

Figure 4: Ratio of combined shear and bending stiffness to bending stiffness with changing width to length ratio of the beam elements for stiffness coefficients as in Equations 79 and 80. The relevance of the shear stiffness decreases with slenderness.

$$g(\rho) \overset{K_\gamma \to \infty}{=} \frac{2\left(2-\rho^2\right) K_f K_e}{8\rho^2 K_f + \left(2-\rho^2\right) K_e} \ . \tag{69}$$

We find in [24] Equation 23:

$$f^*(\rho) = \frac{\rho^2 K_e^* K_f^*}{(2-\rho^2)\left[4(2-\rho^2)K_f^* + \rho^2 K_e^*\right]} \ , \tag{70}$$

$$g^*(\rho) = \frac{\left(\rho^2-2\right) K_e^* K_f^*}{\rho^2\left(K_e^* - 4K_f^*\right) - 2K_e^*} \ , \tag{71}$$

$$h^*(\rho) = K_t^* \left[\frac{\pi}{2} - 2\arccos\left(\frac{\rho}{\sqrt{2}}\right)\right]^2 \tag{72}$$

where for agreement with the micro model, we suggest

$$K_e^* = K_e \ , \tag{73}$$

$$K_f^* = 2K_f \ , \tag{74}$$

$$K_t^* = K_t \ , \tag{75}$$

and in comparison we get

$$f(\rho) \overset{K_\gamma \to \infty}{=} f^*(\rho) \ , \tag{76}$$

$$g(\rho) \overset{K_\gamma \to \infty}{=} g^*(\rho) \ , \tag{77}$$

$$h(\rho) = h^*(\rho) \ . \tag{78}$$

4.2. Relevance of shear deformation

Assuming some simple stiffness coefficients based on a square cross section $A = a^2$ we find for bending and shear stiffness

$$k_\gamma = \frac{EA_\gamma}{l} \Rightarrow K_\gamma \propto a^2\varepsilon^2 \ , \tag{79}$$

$$k_f = \frac{EJ_f}{l} \Rightarrow K_f \propto a^4 \tag{80}$$

with Young's modulus E, effective shear cross section A_γ and second moment of area J_f. From this, we find a relation between bending and shear stiffness to be

$$\frac{K_f}{K_\gamma} \propto \left(\frac{a}{\varepsilon}\right)^2 \propto \left(\frac{a}{l}\right)^2 \ . \tag{81}$$

As can be seen in Figure 4, the shear stiffness becomes relevant for beams with smaller length to width ratios.

5. Discussion and Outlook

A pantographic beam consisting of discrete elements accounting for elongation, bending, shear and torsional deformation has been described. These discrete beam elements consisted of two nodes with deformation measures based on their relative displacement and relative orientation. Through two condensation steps and necessary kinematic constraints an 1D homogenized model of the discrete system's proposed quadratic energy could be found by means of asymptotic expansion and Piola's micro-macro identification. The resulting energy density has dependencies on the stretch and curvature gradient. The bending and shear coefficients from the discrete model can be replaced by one combined coefficient. In the limit for shear stiff beams, the model agrees with an earlier model [4, 24].

A comparison to simulations of the discrete model will follow in future research.

We believe that this approach can pave to the way towards more systematic modeling of metamaterials with beam structures and for structures based on pantographics beams. As the deformation measures are directly linked to discrete 3D beam elements [26, 29], the modeling of materials in 3D space, especially pantographic beams, is an important extension of this approach. This will also enable an advancement of synthesis from bi-pantographic sheets [24] to bi-pantographic blocks based on 3D pantographic structures [35, 36].

6. Acknowledgments

Maximilian Stilz acknowledges funding from Carl-Zeiss Foundation, grant title Skalenübergreifende Charakterisierung robuster funktionaler Materialsysteme.

References

[1] J.-J. Alibert, P. Seppecher, F. dell'isola, Truss Modular Beams with Deformation Energy Depending on Higher Displacement Gradients, Mathematics and Mechanics of Solids 8 (Feb. 2003). doi:10.1177/1081286503008001658.

[2] E. Turco, F. dell'Isola, A. Cazzani, N. L. Rizzi, Hencky-type discrete model for pantographic structures: Numerical comparison with second gradient continuum models, Zeitschrift für angewandte Mathematik und Physik 67 (4) (2016) 85. doi:10.1007/s00033-016-0681-8.
URL https://doi.org/10.1007/s00033-016-0681-8

[3] E. Turco, M. Golaszewski, A. Cazzani, N. L. Rizzi, Large deformations induced in planar pantographic sheets by loads applied on fibers: Experimental validation of a discrete Lagrangian model, Mechanics Research Communications 76 (2016) 51–56. doi:10.1016/j.mechrescom.2016.07.001.
URL http://www.sciencedirect.com/science/article/pii/S0093641316300701

[4] E. Barchiesi, S. R. Eugster, L. Placidi, F. dell'Isola, Pantographic beam: A complete second gradient 1D-continuum in plane, Zeitschrift für angewandte Mathematik und Physik 70 (5) (2019) 135. doi:10.1007/s00033-019-1181-4.
URL https://doi.org/10.1007/s00033-019-1181-4

[5] F. dell'Isola, I. Giorgio, M. Pawlikowski, N. L. Rizzi, Large deformations of planar extensible beams and pantographic lattices: Heuristic homogenization, experimental and numerical examples of equilibrium, Proceedings of the Royal Society A: Mathematical, Physical and Engineering Science 472 (2185) (2016) 20150790. doi:10.1098/rspa.2015.0790.
URL http://rspa.royalsocietypublishing.org/lookup/doi/10.1098/rspa.2015.0790

[6] I. Giorgio, N. L. Rizzi, E. Turco, Continuum modelling of pantographic sheets for out-of-plane bifurcation and vibrational analysis, Proceedings of the Royal Society A: Mathematical, Physical and Engineering Sciences 473 (2207) (2017) 20170636. doi:10.1098/rspa.2017.0636.
URL https://royalsocietypublishing.org/doi/full/10.1098/rspa.2017.0636

[7] H. Abdoul-Anziz, P. Seppecher, Strain gradient and generalized continua obtained by homogenizing frame lattices, Mathematics and Mechanics of Complex Systems 6 (3) (2018) 213–250. doi:10.2140/memocs.2018.6.213.
URL https://msp.org/memocs/2018/6-3/p04.xhtml

[8] J. F. Ganghoffer, H. Reda, A variational approach of homogenization of heterogeneous materials towards second gradient continua, Mechanics of Materials 158 (2021) 103743. doi:10.1016/j.mechmat.2021.103743.
URL https://www.sciencedirect.com/science/article/pii/S0167663621000628

[9] R. Fedele, Approach à la Piola for the equilibrium problem of bodies with second gradient energies. Part II: Variational derivation of second gradient equations and their transport, Continuum Mechanics and Thermodynamics (May 2022). doi:10.1007/s00161-022-01100-z.
URL https://doi.org/10.1007/s00161-022-01100-z

[10] F. dell'Isola, P. Seppecher, J. J. Alibert, T. Lekszycki, R. Grygoruk, M. Pawlikowski, D. Steigmann, I. Giorgio, U. Andreaus, E. Turco, M. Gołaszewski, N. Rizzi, C. Boutin, V. A. Eremeyev, A. Misra, L. Placidi, E. Barchiesi, L. Greco, M. Cuomo, A. Cazzani, A. D. Corte, A. Battista, D. Scerrato, I. Z. Eremeeva, Y. Rahali, J.-F. Ganghoffer, W. Müller, G. Ganzosch, M. Spagnuolo, A. Pfaff, K. Barcz, K. Hoschke, J. Neggers, F. Hild, Pantographic metamaterials: An example of mathematically driven design and of its technological challenges, Continuum Mechanics and Thermodynamics 31 (4) (2019) 851–884. doi:10.1007/s00161-018-0689-8.
URL https://doi.org/10.1007/s00161-018-0689-8

[11] F. dell'Isola, P. Seppecher, M. Spagnuolo, E. Barchiesi, F. Hild, T. Lekszycki, I. Giorgio, L. Placidi, U. Andreaus, M. Cuomo, S. Eugster, A. Pfaff, K. Hoschke, R. Langkemper, E. Turco, R. Sarikaya, A. Misra, M. Angelo, F. D'Annibale, T. Hayat, Advances in Pantographic Structures: Design, Manufacturing, Models, Experiments and Image Analyses, Continuum Mechanics and Thermodynamics 31 (2019) 1231–1282. doi:10.1007/s00161-019-00806-x.

[12] A. Ciallella, D. J. Steigmann, Unusual deformation patterns in a second-gradient cylindrical lattice shell: Numerical experiments, Mathematics and Mechanics of Solids (2022) 10812865221101820doi:10.1177/10812865221101820.
URL https://doi.org/10.1177/10812865221101820

[13] M. Spagnuolo, P. Peyre, C. Dupuy, Phenomenological aspects of quasi-perfect pivots in metallic pantographic structures, Mechanics Research Communications 101 (2019) 103415. doi:10.1016/j.mechrescom.2019.103415.
URL http://www.sciencedirect.com/science/article/pii/S0093641319301525

[14] V. A. Eremeyev, F. dell'Isola, C. Boutin, D. Steigmann, Linear Pantographic Sheets: Existence and Uniqueness of Weak Solutions, Journal of Elasticity 132 (2) (2018) 175–196. doi:10.1007/s10659-017-9660-3.
URL https://doi.org/10.1007/s10659-017-9660-3

[15] V. A. Eremeyev, F. S. Alzahrani, A. Cazzani, F. dell'Isola, T. Hayat, E. Turco, V. Konopińska-Zmysłowska, On existence and uniqueness of weak solutions for linear pantographic beam lattices models, Continuum Mechanics and Thermodynamics 31 (6) (2019) 1843–1861. doi:10.1007/s00161-019-00826-7.
URL https://doi.org/10.1007/s00161-019-00826-7

[16] E. Turco, A. Misra, R. Sarikaya, T. Lekszycki, Quantitative analysis of deformation mechanisms in pantographic substructures: Experiments and modeling, Continuum Mechanics and Thermodynamics 31 (1) (2019) 209–223. doi:10.1007/s00161-018-0678-y.
URL https://doi.org/10.1007/s00161-018-0678-y

[17] M. E. Yildizdag, E. Barchiesi, F. dell'Isola, Three-point bending tests of pantographic blocks: Numerical and experimental investigation, Mathematics and Mechanics of Solids 25 (10) (2020) 1965–1978. doi:10.1177/1081286520916911.
URL https://doi.org/10.1177/1081286520916911

[18] G. Aydin, B. C. Sarar, M. E. Yildizdag, B. E. Abali, Investigating infill density and pattern effects in additive manufacturing by characterizing metamaterials along the strain-gradient theory, Mathematics and Mechanics of Solids 27 (10) (2022) 2002–2016. doi:10.1177/10812865221100978.
URL https://doi.org/10.1177/10812865221100978

[19] A. Ciallella, D. Pasquali, F. D'Annibale, I. Giorgio, Shear rupture mechanism and dissipation phenomena in bias-extension test of pantographic sheets: Numerical modeling and experiments, Mathematics and Mechanics of Solids (2022) 10812865221103573doi:10.1177/10812865221103573.
URL https://doi.org/10.1177/10812865221103573

[20] La Valle, A. Ciallella, G. Falsone, The effect of local random defects on the response of pantographic sheets, Mathematics and Mechanics of Solids (2022) 10812865221103482doi:10.1177/10812865221103482.
URL https://doi.org/10.1177/10812865221103482

[21] M. Spagnuolo, M. E. Yildizdag, X. Pinelli, A. Cazzani, F. Hild, Out-of-plane deformation reduction via inelastic hinges in fibrous metamaterials and simplified damage approach, Mathematics and Mechanics of Solids 27 (6) (2022) 1011–1031. doi:10.1177/10812865211052670.
URL https://doi.org/10.1177/10812865211052670

[22] M. E. Yildizdag, L. Placidi, E. Turco, Modeling and numerical investigation of damage behavior in pantographic layers using a hemivariational formulation adapted for a Hencky-type discrete model, Continuum Mechanics and Thermodynamics (Oct. 2022). doi:10.1007/s00161-022-01154-z.
URL https://doi.org/10.1007/s00161-022-01154-z

[23] E. Barchiesi, F. dell'Isola, M. Laudato, L. Placidi, P. Seppecher, A 1D Continuum Model for Beams with Pantographic Microstructure: Asymptotic Micro-Macro Identification and Numerical Results, in: F. dell'Isola, V. A. Eremeyev, A. Porubov (Eds.), Advances in Mechanics of Microstructured Media and Structures, Vol. 87, Springer International Publishing, Cham, 2018, pp. 43–74.
URL http://link.springer.com/10.1007/978-3-319-73694-5_4

[24] E. Barchiesi, S. R. Eugster, F. dell'Isola, F. Hild, Large in-plane elastic deformations of bi-pantographic fabrics: Asymptotic homogenization and experimental validation, Mathematics and Mechanics of Solids 25 (3) (2020) 739–767. doi:10.1177/1081286519891228.
URL http://journals.sagepub.com/doi/10.1177/1081286519891228

[25] E. Turco, E. Barchiesi, Equilibrium paths of Hencky pantographic beams in a three-point bending problem, Mathematics and Mechanics of Complex Systems 7 (4) (2019) 287–310. doi:10.2140/memocs.2019.7.287.
URL https://msp.org/memocs/2019/7-4/p01.xhtml

[26] E. Turco, E. Barchiesi, I. Giorgio, F. dell'Isola, A Lagrangian Hencky-type non-linear model suitable for meta-

materials design of shearable and extensible slender deformable bodies alternative to Timoshenko theory, International Journal of Non-Linear Mechanics 123 (2020) 103481. doi:10.1016/j.ijnonlinmec.2020.103481.
URL https://www.sciencedirect.com/science/article/pii/S0020746220301485
[27] D. Scerrato, I. A. Z. Eremeeva, T. Lekszycki, N. L. Rizzi, On the effect of shear stiffness on the plane deformation of linear second gradient pantographic sheets, ZAMM - Journal of Applied Mathematics and Mechanics / Zeitschrift für Angewandte Mathematik und Mechanik 96 (11) (2016) 1268–1279. doi:10.1002/zamm.201600066.
URL https://onlinelibrary.wiley.com/doi/abs/10.1002/zamm.201600066
[28] I. Giorgio, N. Rizzi, U. Andreaus, D. Steigmann, A two-dimensional continuum model of pantographic sheets moving in a 3D space and accounting for the offset and relative rotations of the fibers, Mathematics and Mechanics of Complex Systems 7 (2019) 311–325. doi:10.2140/memocs.2019.7.311.
[29] I. Giorgio, V. Varano, F. dell'Isola, N. L. Rizzi, Two layers pantographs: A 2D continuum model accounting for the beams' offset and relative rotations as averages in SO(3) Lie groups, International Journal of Solids and Structures 216 (2021) 43–58. doi:10.1016/j.ijsolstr.2021.01.018.
URL https://www.sciencedirect.com/science/article/pii/S0020768321000263
[30] S. Eugster, C. Hesch, P. Betsch, C. Glocker, Director-based beam finite elements relying on the geometrically exact beam theory formulated in skew coordinates, International Journal for Numerical Methods in Engineering 97 (2) (2014) 111–129. doi:10.1002/nme.4586.
URL https://onlinelibrary.wiley.com/doi/abs/10.1002/nme.4586
[31] J. Harsch, G. Capobianco, S. R. Eugster, Finite element formulations for constrained spatial nonlinear beam theories, Mathematics and Mechanics of Solids 26 (12) (2021) 1838–1863. doi:10.1177/10812865211000790.
URL https://doi.org/10.1177/10812865211000790
[32] L. Greco, An iso-parametric G1 -conforming finite element for the nonlinear analysis of Kirchhoff rod. Part I: The 2D case, Continuum Mechanics and Thermodynamics 32 (2020) 1473–1496. doi:10.1007/s00161-020-00861-9.
URL https://ui.adsabs.harvard.edu/abs/2020CMT....32.1473G
[33] I. Giorgio, A discrete formulation of Kirchhoff rods in large-motion dynamics, Mathematics and Mechanics of Solids 25 (5) (2020) 1081–1100. doi:10.1177/1081286519900902.
URL https://doi.org/10.1177/1081286519900902
[34] Wolfram Research, Inc., Mathematica, Version 13.1 (2022).
URL https://www.wolfram.com/mathematica
[35] M. Stilz, D. Plappert, F. Gutmann, S. Hiermaier, A 3D extension of pantographic geometries to obtain metamaterial with semi-auxetic properties, Mathematics and Mechanics of Solids 27 (4) (2022) 673–686. doi:10.1177/10812865211033322.
URL https://doi.org/10.1177/10812865211033322
[36] M. Stilz, F. dell'Isola, I. Giorgio, V. A. Eremeyev, G. Ganzenmüller, S. Hiermaier, Continuum models for pantographic blocks with second gradient energies which are incomplete, Mechanics Research Communications 125 (2022) 103988. doi:10.1016/j.mechrescom.2022.103988.
URL https://www.sciencedirect.com/science/article/pii/S0093641322001203

Appendix A. Diverging energy contributions

From the expansion in Section 3.4 there are contributions that scale with ε^{-1} and therefore diverge in the limit of small ε from shear and bending energy:

$$W_{tot}^{(-1)} = W_\gamma^{(-1)} + W_f^{(-1)} \,, \tag{A.1}$$

$$W_\gamma^{(-1)} = \frac{K_f^2 K_\gamma}{4K_f + K_\gamma}\left[\left(\pi - 4\arccos\left(\frac{\rho}{\sqrt{2}}\right) + 4\vartheta - 4\psi_0^{P^-}\right)^2 + \left(\pi - 4\arccos\frac{\rho}{\sqrt{2}} + 2\psi_0^{P^-} + 2\psi_0^{P^+}\right)^2\right] , \tag{A.2}$$

$$W_f^{(-1)} = \frac{K_f K_\gamma^2}{4K_f + K_\gamma}\left[\left(\pi - 4\arccos\left(\frac{\rho}{\sqrt{2}}\right) + 4\vartheta - 4\psi_0^{P^-}\right)^2 + \left(\pi - 4\arccos\frac{\rho}{\sqrt{2}} + 2\psi_0^{P^-} + 2\psi_0^{P^+}\right)^2\right] . \tag{A.3}$$

Solutions for $\psi_0^{P^-}, \psi_0^{P^+} \in \mathbb{R}$ then bring the constraints

$$\pi - 4\arccos\frac{\rho}{\sqrt{2}} + 4\vartheta - 4\psi_0^{P^-} \stackrel{!}{=} 0 \tag{A.4}$$

$$\Rightarrow \psi_0^{P^-} = \vartheta - \arccos\left(\frac{\rho}{\sqrt{2}}\right) + \frac{\pi}{4} \,, \tag{A.5}$$

$$\pi - 4\arccos\frac{\rho}{\sqrt{2}} + 2\psi_0^{P^-} + 2\psi_0^{P^+} \stackrel{!}{=} 0 \tag{A.6}$$

$$\Rightarrow \psi_0^{P^+} = \vartheta + \arccos\left(\frac{\rho}{\sqrt{2}}\right) - \frac{\pi}{4} \,. \tag{A.7}$$

There are also contributions for $W_\gamma^{(0)}$ and $W_f^{(0)}$ which are lengthy differential equations of $\vartheta(s)$, $\rho(s)$, $\psi_0^{P^\pm}(s)$ and $\psi_1^{P^\pm}(s)$ but with Equations A.5 and A.7 they fulfill

$$W_\gamma^{(0)} = 0 \,, \tag{A.8}$$

$$W_f^{(0)} = 0 \,. \tag{A.9}$$